Santiago, 25 June 2018

Experimental and computational characterization of the interaction between gold nanoparticles and PAMAM dendrimers

M.B. Camarada[1]*, J. Comer[2]*, H. Poblete[3], E.R. Azhagiya Singam[2], V. Marquez-Miranda[4,5], C. Morales-Verdejo[1], F.D. Gonzalez-Nilo[5]

[1]Centro de Nanotecnología Aplicada, Facultad de Ciencias, Universidad Mayor, Camino la Pirámide 5750, Huechuraba, Santiago, Chile

[2]Nanotechnology Innovation Center of Kansas State, Institute of Computational Comparative Medicine, Department of Anatomy and Physiology, Kansas State University, 1800 Denison Ave, Manhattan, Kansas, KS 66506, United States of America

[3]Centro de Bioinformática y Simulación Molecular, Facultad de Ingeniería; Nucleo Científico Multidiciplinario-DI; Millennium Nucleus of Ion Channels-Associated Diseases (MiNICAD), Universidad de Talca, 2 Norte 685, Casilla 721, Talca, Chile

[4]Current address: uBiome SpA, Av. Santa María 2810, Providencia, Santiago, Chile.

[5]Universidad Andrés Bello, Center for Bioinformatics and Integrative Biology (CBIB), Facultad de Ciencias de la Vida, Av. República 330, Santiago, Chile

Abstract

Dendrimers provide a means to control the synthesis of gold nanoparticles and stabilize their suspensions. However, design of improved dendrimers for this application is hindered by a lack of understanding how the dendrimers and synthesis conditions determine nanoparticle morphology and suspension stability. In the present work, we evaluate the effect of polyamidoamine (PAMAM) dendrimers terminated with different functional groups (–OH or $–NH_3^+$) and different synthesis conditions on the morphology of the resulting gold nanoparticles and their stability in solution. We leverage molecular dynamics simulations to identify the atomic interactions that underlie adsorption of PAMAM dendrimers to gold surface and how the thermodynamics of this adsorption depends on the terminal functional groups of the dendrimers. We find that gold nanoparticles formed with hydroxyl-terminated PAMAM (PAMAM–OH) rapidly aggregate, while those formed with PAMAM–NH_3^+ are stable in solution for months of storage. Synthesis under ultrasound sonication is shown to be more rapid than under agitation, with sonication producing smaller nanoparticles. Free-energy calculations in molecular dynamics simulations show that all dendrimers have a high affinity for the gold surface, although PAMAM–OH and its oxidized aldehyde form (PAMAM–CHO) have a greater affinity for the nanoparticle surface than PAMAM–NH_3^+. While adsorption of PAMAM–OH and PAMAM–CHO has both favorable entropy and enthalpy, adsorption of PAMAM–NH_3^+ is driven by a strong enthalpic component subject to an unfavorable entropic component.

Keywords

dendrimers, PAMAM, gold nanoparticles, adaptive biasing force, sonication

email: maria.camarada@umayor.cl, jeffcomer@ksu.edu

Introduction

Metal nanoparticles have attracted great interest because of their use in a wide range of applications such as medicine[1], microelectronics[2], catalysis[3] and biotechnology[4]. Due to their high surface-area-to-volume ratios, the physicochemical properties of nanoparticles strongly depend on their size and morphology, in contrast to bulk materials[5-7]. Some nanosized catalysts have a strong tendency to agglomerate, diminishing their utility[8]. Stabilizers based on polymers, surfactants and chelating agents serve to attenuate their propensity to agglomerate[9], acting as ‘‘armor’’ around the metal nanoparticles. Dendrimers have been shown to serve as patterns for synthesis and stabilizers of metal nanoparticles[10]. These hyper-branched polymers are globular nanoscale macromolecules characterized by a strictly controlled structure, definite molecular weight, near monodispersity, and biocompatibility[11]. They have a branched structure, consisting of a core, a controllable number of branching levels and terminal functional groups[12]. Polyamidoamine (PAMAM) dendrimers are an important class of dendrimers with repeating amide functionalities, tertiary amines at the branching points and primary amines at the termini of the branches, and have been used with increasing frequency in the synthesis of nanoparticles[13]. At neutral pH, primary external amines typically remain protonated[14-15], allowing nonspecific ionic interaction with biological and inorganic interphases[10, 16]. The termini of the branches of PAMAM type dendrimers can also be functionalized with other chemical groups such as carboxylic acids or hydroxyls, which may impact the reactivity and solubility of the polymer.

Among the different sizes of dendrimers, generation 4 has been reported to be an excellent platform for the synthesis of different type of nanoparticles such as Pt[17], Pd[10] and Cu[18]. Gold nanoparticles have also attracted wide attention in different fields mainly because of its chemical inertness[19], facile synthesis[20-21], and biocompatibility[22]. To date, the main subject of several studies has been the production of stable gold nanoparticles in the presence of PAMAM dendrimers[23-24]. Both PAMAM G4–NH_3^+ (PAMAM–NH_3^+) and –OH (PAMAM–OH) have been successfully applied for the synthesis of gold nanoparticles with sizes starting from approximately 2 nm[25].

Different methods for the synthesis of gold nanoparticles have been developed. In the case of the dendrimer-assisted synthesis, the most common methodology involves the application of a gold salt like $HAuCl_4$, which is mixed with the dendrimer in aqueous solution to enable the interaction between gold and the coordination sites of the polymer. The complexation starts with the interaction of the $AuCl_4^-$ ions with the terminal groups of the dendrimer[26] through electrostatic interactions, covalent bonds formation, and/or physical

complexation[27-28], displacing water molecules coordinated to the terminal sites. After mixing, a reducing agent like ascorbic acid, sodium citrate or sodium borohydride is added to reduce the Au(III) centers to metallic gold, as the following semi-reaction represents:

$$AuCl_4^- + 3e^- \rightarrow Au + 4Cl^- \quad (1)$$

Dendrimers of different generations can be applied as patterns for the synthesis of gold nanoparticles. High generation dendrimers (G5 and above) have densely packed branches and take on a roughly spherical shape, while lower generation dendrimers (G0-G4) adopt more disc-like conformations with interior solvent-filled voids. Major differences have been found in the mechanism of nanoparticle stabilization by higher and lower generation dendrimers. Previous studies reported that higher generations adopt a globular three-dimensional structure, providing internal coordination sites that can act as an effective protective shell for the formation of nanoparticles inside the dendrimer[29]. On the other hand, lower generation dendrimers (G0–G4) stabilize gold nanoparticles by forming a coordination shell of multiple dendrimer molecules around the nascent nanoparticles[30-35], as Figure 1 schematically illustrates. Nanoparticles are first formed at the surface of the dendrimer and are subsequently capped by contact with multiple dendrimer molecules.

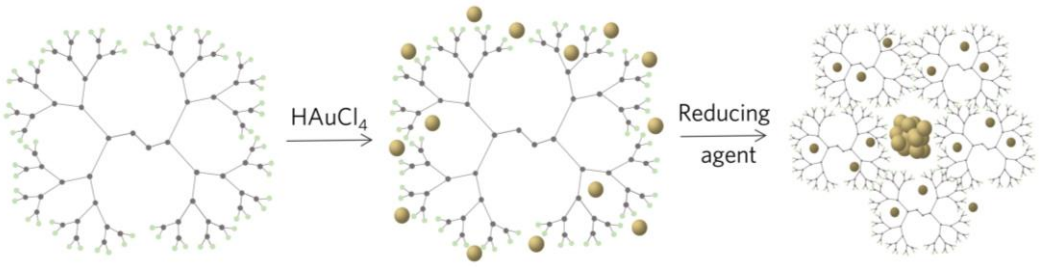

Figure 1: Schematic synthesis of gold nanoparticles using PAMAM G4.
● $-NH_3^+$ or –OH in PAMAM–NH_3^+ and PAMAM–OH, respectively.

The effect of PAMAM surface end groups on the architecture of the nanoparticles has been also investigated[36]. Gold nanoparticles synthesized in the presence of PAMAM–OH are more prone to aggregation than those stabilized by PAMAM–NH_3^+[37], due to the premature reduction of $AuCl_4^-$ ions[38]. Nanoparticles synthetized with PAMAM–OH coalesce almost instantaneously after formation, showing low stability in comparison to PAMAM–NH_3^+[39]. *Esumi* and coworkers described the strong capacity of hydroxyl-modified dendrimers to spontaneously reduce metals without the addition of any reducing agent[40]. These “sugar

ball" dendrimers showed an ability to reduce Au(III) to metal nanoclusters through the several –OH terminal groups that were thereby oxidized to aldehydes.

Currently, there is a lack of understanding of the atomic level interactions that give different terminal groups their capacities for gold nanoparticle stabilization, impeding the rational design of improved stabilizers. Hence, here we perform experiments to compare the action of PAMAM–NH_3^+ and PAMAM–OH dendrimers as stabilizers in gold nanoparticle synthesis, leveraging molecular dynamics simulation to reveal the interaction between gold nanoparticles and these dendrimers at the atomic level.

Experimental

Reagents

Reagents were of analytical grade of the highest commercially available purity and were used as received. Fourth generation amino (PAMAM–NH_3^+) and hydroxyl terminated (PAMAM–OH) PAMAM dendrimers with an ethylenediamine core were purchased from Sigma-Aldrich as a 10% solution in methanol. Gold (III) chloride hydrate, $HAuCl_4 \cdot 3H_2O$, was purchased from Sigma-Aldrich. Trisodium citrate dihydrate was obtained from Merck. Solutions were prepared with ultrapure water of resistivity not less than 18 MΩ cm (Milli-Q, USA).

Synthesis of Dendrimer-Encapsulated Au Nanoclusters

The preparation of the gold nanoparticles with the hydroxyl terminated PAMAM (PAMAM–OH|Au) and similar nanoparticles with the amino terminated dendrimer (PAMAM–NH_3^+|Au) was performed according to the literature with some modifications[41]. Most of the studies have employed stirring procedures for the synthesis. In the present work, two methodologies of syntheses were applied: magnetic stirring and ultrasound sonication using an Elmasonic S30H ultrasound bath. Briefly, 0.5 mL PAMAM (0.1 mM) was stirred (40 min) or sonicated in an Eppendorf tube (10 min) with 0.5 mL of $HAuCl_4$. Different gold concentrations were selected to study the effect on the particle size. The selected gold concentrations were between 0.3 and 2.4 mM. Then, the reducing agent, 0.5 mL of sodium citrate with a concentration equal to the gold concentration used for each sample, was added to the resulting mixture. The mixtures were stirred for 4 hours or sonicated for 30 min. Beakers and Eppendorf tubes were covered with aluminum foil to avoid gold salt decomposition by light.

Characterization was made immediately after the end of the synthesis by UV-vis spectroscopy.

Characterization

UV-visible spectra were recorded with a Jasco V-630 UV-visible spectrophotometer. All measurements were taken at room temperature. High Resolution Scanning electron microscopy (HR-SEM) was carried out using a FEI equipment model INSPECT-F50. Atomic force microscopy (AFM) was performed with a Bruker, Innova AFM.

Construction of Atomistic Models

In order to study the structural interaction between PAMAM–NH_3^+ and PAMAM–OH and gold nanoparticles, molecular models were constructed using the program VMD 1.9.2[42]. Considering the experimental evidence related to the spontaneous oxidation of the hydroxyl terminal groups of PAMAM–OH to aldehydes in the presence of Au(III), the oxidized species, PAMAM–CHO, was also considered in the simulations. To reduce the computational expense and obtain sufficient sampling, we used PAMAM G0 as a model for PAMAM G4. Although the surface of PAMAM G4 has a higher density of terminal groups than PAMAM G0, the identical chemical nature of the terminal groups of the two dendrimers suggests that simulations with G0 should be sufficient to identify particular interactions and their strength. Atomic interaction parameters for PAMAM–NH_3^+, PAMAM–OH, and PAMAM–CHO were obtained consistent with the CHARMM General Force Field (CGenFF)[43] using the ParamChem website (http://www.paramchem.org)[44-45]. Conventional classical MD is incapable of reproducing protonation and deprotonation of certain groups during the simulation. Although simulation methods for constant pH ensembles exist, they introduce many practical difficulties in performing the simulations. Therefore, to approximate experimental conditions, each one of the 4 terminal amines in the molecular model of the dendrimer was set to a positive charge of +1*e* (PAMAM–NH_3^+).

The gold nanoparticle was approximated as a gold {111} surface (6.25×6.25 nm^2), constructed with a lattice parameter of 2.93 Å[46], according to the model reported previously by *Wright* and coworkers[47] based on first-principles calculations. The *Wright* model includes dynamic polarization of gold atoms, represented by virtual particles that are fixed to each gold atom and reorient according to changes in the local electric field, as well as virtual interaction sites to ensure the adsorption of species on top of the gold {111} surface atoms rather than in their interstices. Gold atoms were assigned with a charge of −0.300*e*, while

the virtual particles carried the opposite charge. The simulation box was periodic along all three axes and was built taking into account the gold surface dimension, placing water molecules below and above the gold layer to give an equilibrium height of approximately 6 nm along the *z* axis, as Figure 2a shows.

Molecular Dynamics (MD) Simulations

MD simulations were run using an isobaric-isothermal (NPT) ensemble, where the number of particles, the pressure and the temperature were held constant, using the computational code NAMD 2.11[48]. A Langevin thermostat was employed to keep a mean temperature of 300 K, and the Langevin piston[49] method was used to maintain a mean pressure of 1 atm (101.325 kPa). Non-bonded interactions were calculated using particle-mesh Ewald full electrostatics[50] (grid spacing < 1.2 Å). Long- and short-range electrostatic interactions were calculated every 2 steps using a multiple-time stepping scheme. A smooth 0.8–0.9 nm cutoff of van der Waals forces was employed. The TIP3P water model[51] standard to the CHARMM force field[52-53] was used. The equations of motion were integrated with a 2.0 fs time step, with SETTLE[54] and RATTLE[55] algorithms used to constrain the geometry of the water molecules and the length of covalent bonds to hydrogen atoms.

All systems were independently subjected to 2000 steps of energy minimization followed by 5 ns of equilibration simulation before beginning the free-energy calculations. All simulation systems had the shape of rectangular prisms, and periodic boundary conditions were enforced in all three directions. Suitable numbers of Cl^- ions were added to the PAMAM–NH_3^+ simulation system to obtain neutrality. The area of the systems in the plane of the gold surface (the *xy* plane) was kept fixed, and the Langevin piston acted only at the *z* axis. VMD 1.9.2 software was used to visualize and analyze the simulations and to perform molecular rendering[42].

Free-energy Calculations

The adaptive biasing force method[56-58] was used to calculate the adsorption free energy of the dendrimers, beginning from equilibrated system configurations. In the case of PAMAM**–**OH and PAMAM**–**CHO, only one transition coordinate was selected: $Z=z$(dendrimer)-z(Au) to sample the distance from the center of mass of the dendrimer to the gold surface. For PAMAM**–**NH_3^+, two transition coordinates were used to more fully describe the free energy of the system and obtain adequate sampling of conformational changes of the dendrimer. These coordinates were: the distance between the dendrimer and gold surface

Z=*z*(PAMAM–NH_3^+)-*z*(Au) and dz, defined as the *z*-displacement between the core of the dendrimer and the terminal amino groups of PAMAM, as depicted in Figure 2b.

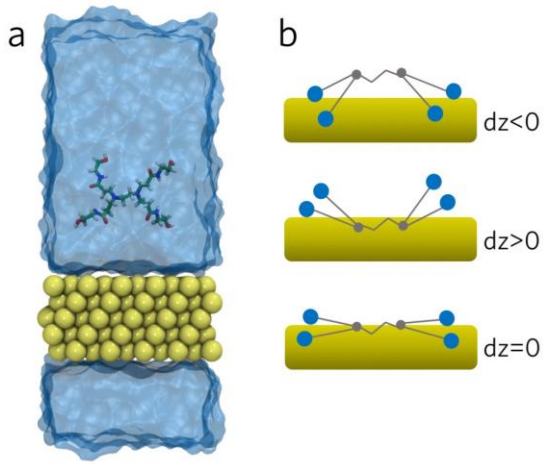

Figure 2: (a) Schematic view of the simulation box where explicit water molecules are represented as a transparent blue surface and gold atoms are depicted by yellow spheres. The dendrimer is depicted in a bonds representation with H, C, N, and O atoms shown in white, green, blue, and red, respectively. For clarity, the interstitial surface particles and charged particles for polarizability prescribed by the *Wright* model for gold {111} are not shown. (b) Depiction of the second transition coordinate (dz) applied to the PAMAM–NH_3^+ system.

When the dendrimer is near the surface, negative values of dz correspond to contact between the terminal groups of the dendrimer and the gold surface, while positive dz values indicate contact between the core and the surface. Finally values equal to zero are linked to an extended configuration on gold. The adaptive biasing force methodology was implemented through the Colvars module[59] of NAMD 2.11[48]. For PAMAM–OH and PAMAM–CHO, the collective variable Z was sampled on a single window $2 \geq Z \leq 20$ Å, while for PAMAM–NH_3^+, a single window of $3.7 \leq Z \leq 20$ Å and $-5 \leq dz \leq 5$ Å was used. For each dendrimer, the free-energy calculations constituted a simulation time of at least 3000 ns.

Results and discussion

PAMAM–NH_3^+ and PAMAM–OH Encapsulated Gold Nanoparticles

With the aim of studying the effect of $HAuCl_4$ concentration on the final particle size, different molar concentration ratios of PAMAM:$HAuCl_4$ were used. Once the PAMAM and gold (III) solution were mixed, the pale-yellow color of the solution changed spontaneously to light pink at ratios higher than 1:15 in the case of PAMAM–NH_3^+ and to purple at ratios higher than 1:3 in the case of PAMAM–OH, as Figure S1 displays. The capacity of hydroxyl terminated dendrimers to spontaneously reduce metals without the addition of an additional reducing agent has previously been reported. “Sugar ball” dendrimers, first reported by *Esumi* and coworkers[40], were able to reduce gold (III) to metal nanoclusters through the several –OH terminal groups that can be oxidized to carbonyl moieties. PAMAM–NH_3^+ has also been reported as a reducer of gold cations[60-61], demonstrated by the change of color of the solution without the addition of another reducing agent. However, its reducing power is lower than the hydroxyl terminated PAMAM, consistent with the larger concentration of gold needed to see the pink color in the solution as Figure S1 shows. This evidence is in agreement with reports describing that hydroxyl terminal groups trigger the automatic reduction of cationic gold without the presence of a reducing agent, causing the spontaneous oxidation of the terminal groups of the dendrimer[40].

After the mixing time, a mild reducing agent was added to each mixture (sodium citrate). In concentrations of $HAuCl_4$ higher than ratio 1:9, the color of the PAMAM–NH_3^+ reaction changed to fuchsia while the PAMAM–OH reactor changed to deep purple indicating that PAMAM–Au complexes were formed. At the end of the reaction, all samples were characterized via UV-vis spectroscopy, shown in Figure 3. As the concentration of gold increased, the UV-vis spectra showed a broad and intense band, between 520 nm and 540 nm, characteristic of zero-valent gold particles not covalently bonded to the dendrimer[62-63].

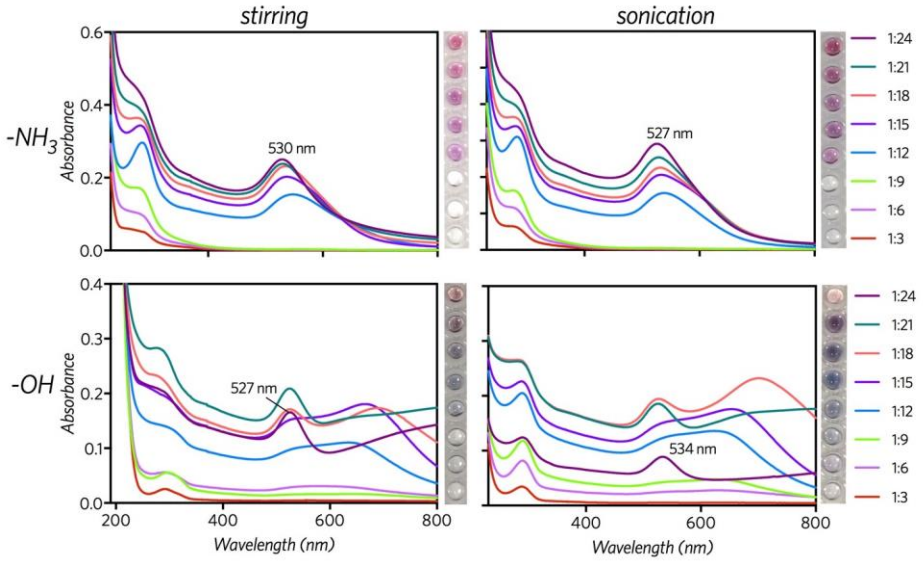

Figure 3: UV-vis spectra of gold nanoparticles synthesized with PAMAM–NH_3^+ (0.5 mL 0.1 mM) and PAMAM–OH (0.5 mL 0.1 mM) with different PAMAM:$HAuCl_4$ molar concentration ratios. 0.5 mL of sodium citrate in equimolar concentration with $HAuCl_4$ was added to each tube. Photographs of the corresponding suspensions are shown to the right of the plots to illustrate their colors.

In the case of PAMAM–OH, at PAMAM:Au ratios from 1:6 to 1:18, there is a broad and undefined band at long wavelengths related to high dispersion. The first zone corresponding to the peak around 530 nm was assigned to the formation of gold nanoparticles. The second peak at longer wavelength, approximately 650 nm, is related to the coagulation of the samples[37]. At higher concentration, the peak at shorter wavelength was more defined, evidence of lesser dispersion, while the lower energy peak progressively vanished, indicating minor agglomeration. As the concentration rises, more of the external hydroxyl sites react with gold and are oxidized to carbonyl groups. Then, not all the gold atoms are immediately reduced by the –OH moieties. In this way, some of the Au(III) atoms are stabilized and capped by the dendrimer shell, diminishing the tendency to coalesce.

Considering *Mie* theory that relates the particle diameter to the maximum of the absorption peak, it can be stated that color is a function of the size and shape of the metal nanoparticles[64-65]. In the case of PAMAM–NH_3^+ and independent of whether stirring or sonication was used, as the concentration of gold increased, the band associated with metallic gold was shifted to higher energy indicating that the size of the nanoparticles decreased. As Figure 3 shows, at the highest ratio of gold (1:24) the PAMAM–NH_3^+ spectra shows a peak at 530 nm and at 527 nm, while PAMAM–OH has its maximum at 527 nm and

534 nm, for stirring and sonication methodologies, respectively. Both methodologies resulted in stronger zero-valent gold bands for PAMAM–NH_3^+.

SEM microphotographs were taken for nanoparticles synthesized with a 1:12 PAMAM:Au ratio and the ultrasound methodology (Figure 4), confirming the greater agglomeration of the PAMAM–OH sample. Particle size measurements with the software ImageJ[66] showed that PAMAM–NH_3^+ give rise to smaller gold nanoparticles (~2 nm) than PAMAM–OH (~4 nm). The size distribution analysis suggested mean sizes near 7 nm for PAMAM–NH_3^+ and 10 nm for PAMAM–OH. AFM characterization of nanoparticles synthesized with PAMAM–NH_3^+ at a 1:12 PAMAM:Au ratio displayed an average particle height of 2.1 nm as Figure S2 shows.

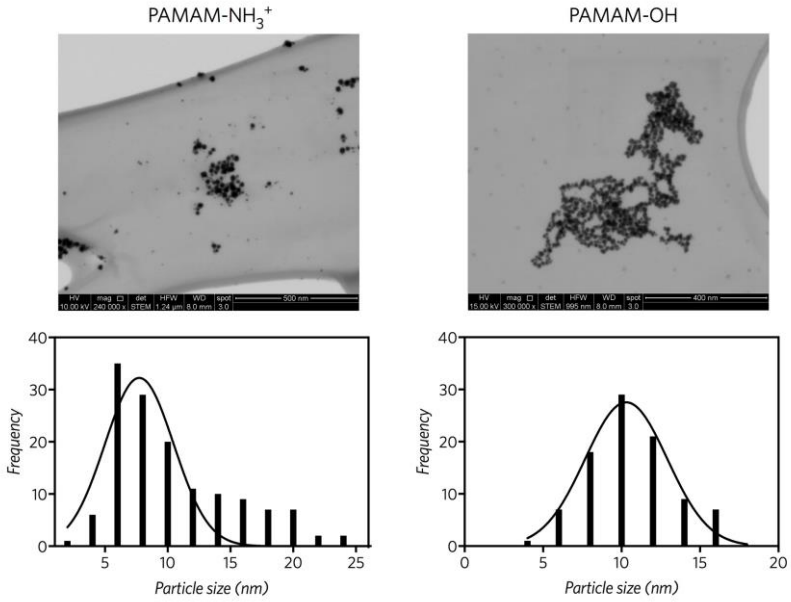

Figure 4**:** SEM microphotographs of gold nanoparticles synthesized with PAMAM–NH_3^+ and PAMAM–OH at a PAMAM:Au ratio of 1:12, using the ultrasound methodology.

Considering these results, PAMAM–NH_3^+ is an appropriate stabilizer for the synthesis of smaller gold nanoparticles. PAMAM–NH_3^+ appears to be a more efficient candidate for gold nanoparticle stabilization at the synthesis conditions applied in this work, owing to less agglomeration and a stronger zero-valent gold band compared to PAMAM–OH. On the other hand, for PAMAM-NH_3^+, the sonication method turned out to be faster and simpler than the stirring methodology and gave rise to smaller nanoparticles.

When the UV-vis profiles were analyzed, a second, high-energy band could be distinguished at 285 nm for PAMAM–NH_3^+ and at 286 nm for PAMAM–OH (Figure 3). Figure 5 shows the spectra of solutions of PAMAM dendrimers alone, together with the spectra of

gold solution alone. Before reduction, $AuCl_4^-$ has a strong peak at 220 nm and a shoulder at 290 nm due to the ligand to metal charge transfer. PAMAM–NH_3^+ and PAMAM–OH show weak absorption bands at 280 nm and 284 nm, respectively. Once the reducing agent was added, the band at 220 nm disappeared indicating that the contribution of Au(III) to the spectra can be discarded because of the excess of the reducing agent. Then, the intense band at low wavelengths of PAMAM–NH_3^+|Au and PAMAM–OH|Au can be assigned in one part to the ligand to metal charge transfer (LMCT), which is similar to previous studies performed with chitosan and Au(III)[67], and also, to the oxidation of the terminal groups of the dendrimers, as demonstrated by *Giorgetti* and coworkers[68].

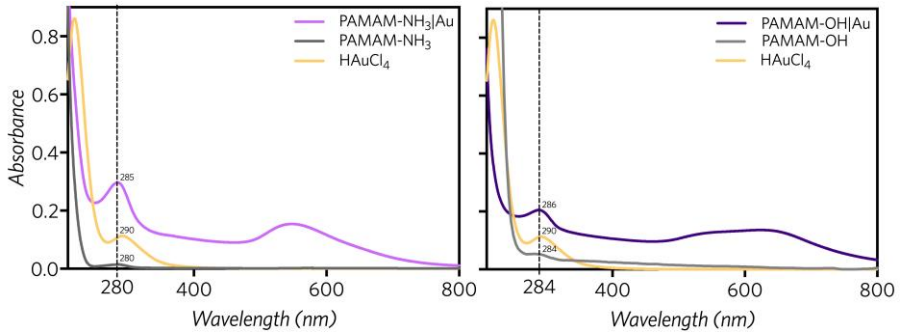

Figure 5: UV-vis spectra of PAMAM–NH_3^+ (0.1 mM), PAMAM–OH (0.1 mM), $HAuCl_4$ (0.1 mM) and gold nanoparticles synthetized with both dendrimers.

Most synthesis of PAMAM nanoparticles are based on the agitation method. Nonetheless, the sonication procedure takes less time, requires simpler mounting, and results in smaller gold nanoparticles. PAMAM–NH_3^+ samples were stable for 3 months at room temperature, with no signs of alteration. On the contrary, PAMAM–OH samples showed precipitation of black aggregates after 48 h, confirming the instability of nanoparticles formed with this dendrimer. Considering this evidence, PAMAM–OH does not operate as an effective protective system, being unable to prevent coalescence, at least under the conditions considered here. The better suspension stability of PAMAM–NH_3^+ coated nanoparticles is likely due to the electrostatic repulsion of the NH_3^+ terminal groups inhibiting aggregation.

Molecular Simulation and Free Energy Profiles of the Interaction of PAMAM and gold. Free-energy calculations were performed to study the binding of PAMAM to a gold nanoparticle surface at the atomic level. Previous studies reported by *Mandal* and coworkers[69], identified the gold {111} facet as the most stable when interacting with PAMAM dendrimers. Therefore, a gold {111} surface as modeled by the force field of *Wright* et al.[47]

was selected as an approximation for the gold nanoparticle. The free-energy calculations were implemented in simulation boxes with explicit solvent, placing the center of mass of the dendrimer at a starting distance of 10 Å from the surface, as Figure 2a shows. The adaptive biasing force[56-58] methodology was used to determine the free energy. In the case of PAMAM–NH_3^+, the use of one transition coordinate resulted in poor sampling and therefore, inadequate description of the interaction energy. Two collective variables were defined to improve sampling and description of conformational states. The first collective variable, Z, was defined as the distance between the center of mass of the dendrimer and the plane passing through the first layer of gold atoms. The second coordinate (dz) was defined as the projected distance between the core of the dendrimer and the terminal amino groups of PAMAM–NH_3^+, as Figure 2b describes. Both coordinates were subjected to multiple walker adaptive biasing force methods[70-71]. For the systems PAMAM–OH and PAMAM–CHO, only the coordinate Z appeared to be necessary to obtain adequate sampling of different PAMAM conformations.

Figure 6 illustrates the free-energy landscape (potential of mean force, PMF) for PAMAM–NH_3^+ in two dimensions: coordinate Z and dz and conformations of the dendrimer in six different areas of the free-energy plot.

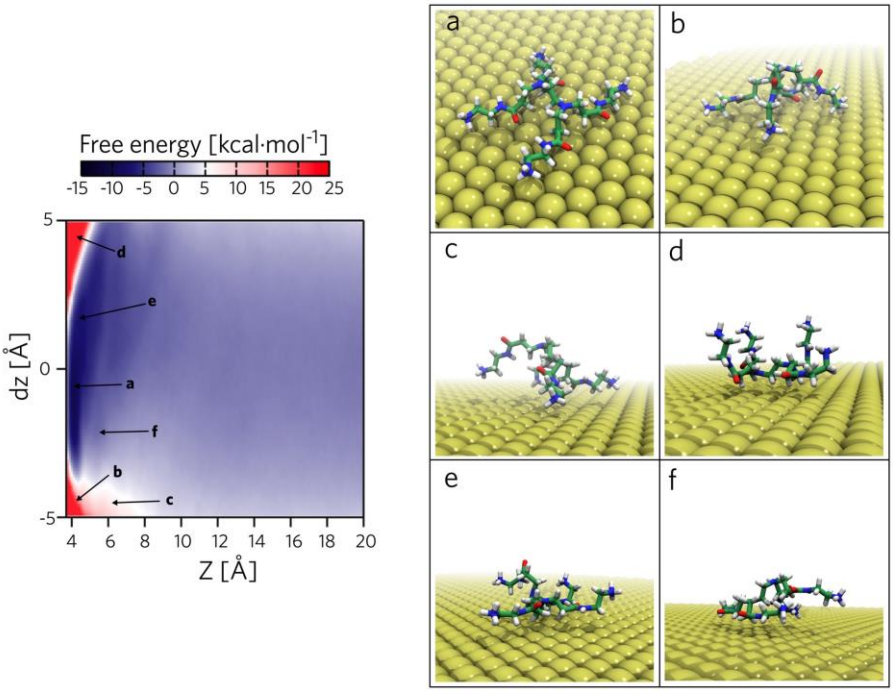

Figure 6: 2D free-energy plot for PAMAM–NH_3^+ and conformations associated to the letters marked in the free energy graph.

The blue regions correspond to high affinity interaction between the dendrimer and the gold surface, while the red areas are related to unfavorable interactions. The global free energy minimum is located at point (a), where the strongest interaction between the dendrimer and the gold {111} surface was registered, with Z ≈ 4.1 Å and dz ≈ -0.95 Å. As Figure 6a depicts, all the branches and terminal groups of the dendrimer are in contact with the surface, favoring the interaction with gold. The ethylenediamine core, carbonyl sites of amido groups and terminal $–NH_3^+$ moieties are located in direct interaction with the Au atoms. As illustrated in Figure 2b, there are three different cases for the values for the coordinate dz corresponding to different orientations of the terminal groups. Figure 6b represents a local maximum (Z ≈ 4.7 Å and dz ≈ −4.15 Å) associated to dz less than zero and Z near to the limiting value −5 Å. This structure has only four anchoring points to gold, and has a high degree of stress. Likewise, Figure 6d which represents the opposite orientation: dz values greater than zero, and Z close to the limiting value 5 Å. This conformation is also very strained, leaving terminal $–NH_3^+$ groups as far as possible from the surface, diminishing the contact points with the gold surface, and therefore, generating a thermodynamically unstable structure. Figure 6c shows a more stable conformation in comparison to (b), where the structure is less strained, and the orientation of the dendrimer allows the interaction of three of the terminal groups and part of the core. It is interesting to note when the dendrimer is at an intermediate distance from the surface (Z>5 Å), conformations like that in Figure 6e, with the core relatively closer to the surface than the terminal groups and dz>0, are more favorable than those with dz<0, a trend that reverses at short distances (Z<4.5 Å).

Figure 7 shows the free-energy landscape for PAMAM–OH as a function of the distance between the dendrimer and the gold surface (i.e., as a function of the coordinate Z). Figure 7a depicts the typical conformation of the global minimum. Like PAMAM–NH_3^+, the most stable interaction is related to a planar conformation (a), that maximizes the contact between the functional groups of the dendrimer and the gold {111} surface. Figure 7b and c show typical conformations at local features in the free-energy landscape of PAMAM–OH. Conformation (c) displays the formation of the first contact between the dendrimer and gold surface through a terminal hydroxyl group, while (b) shows a more advanced state of coordination, where three branches of PAMAM are already in contact with gold.

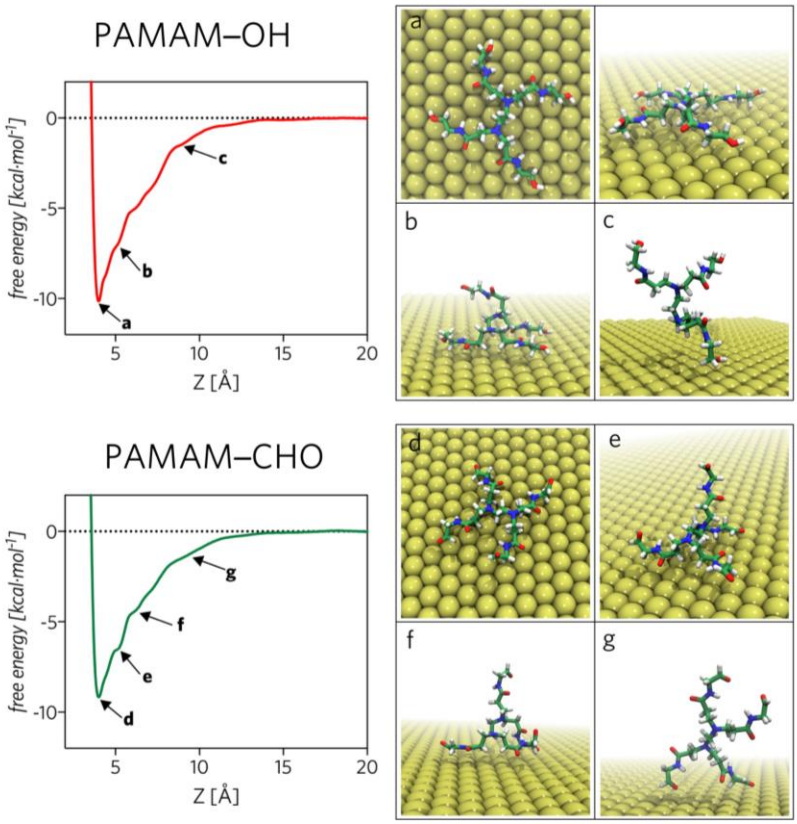

Figure 7: 1D free-energy profiles of PAMAM–OH and PAMAM–CHO along the transition coordinate Z and snapshots of the conformations of PAMAM–OH/Au and PAMAM–CHO/Au , corresponding to the letters marked in the plots of energy.

The free-energy profile was also determined for the oxidized PAMAM–OH system: PAMAM–CHO, with terminal aldehyde groups. As can be seen in Figure 7, the free-energy profile was similar to that obtained for PAMAM–OH. The lowest free energy (Figure 7d), was associated to an extended geometry, favoring the contact between the core, amido and terminal groups with gold, similar to the PAMAM–OH and $–NH_3^+$ systems. At Z ≈ 5.25 Å, PAMAM–CHO exhibits a marginal local minimum (e), which is associated with three branches of the dendrimer making contact with the surface. Overall the free-energy minimum of PAMAM–CHO is shallower than that of PAMAM–OH, implying weaker adsorption. At a distance Z ≈ 11 Å, PAMAM–CHO adopts conformation (g), shown in Figure 7g, with two branches of the dendrimer making contact with gold. Such a conformation was observed in 70% of the simulation frames at this distance. At the same Z value, PAMAM–OH has only one branch contacting the surface; however, the interaction energy is similar (-0.5 kcal·mol^{-1}).

To allow direct comparison to the results with PAMAM–OH and PAMAM–CHO, the two-dimensional potential of mean force of PAMAM–NH_3^+ was integrated to a one-dimensional potential of mean force. Figure 8a compares the free-energy landscape of the three dendrimers as a function of Z. In all cases, the free-energy reaches a plateau with Z values greater than 13 Å, and rapidly decreases as the distance between the dendrimer and the surface diminishes, reaching the global minima at approx. 4.1 Å, being slightly greater for PAMAM–NH_3^+ (4.15 Å). At distances shorter than that, the free-energy rapidly increases due to steric interactions preventing the dendrimer from penetrating the surface.

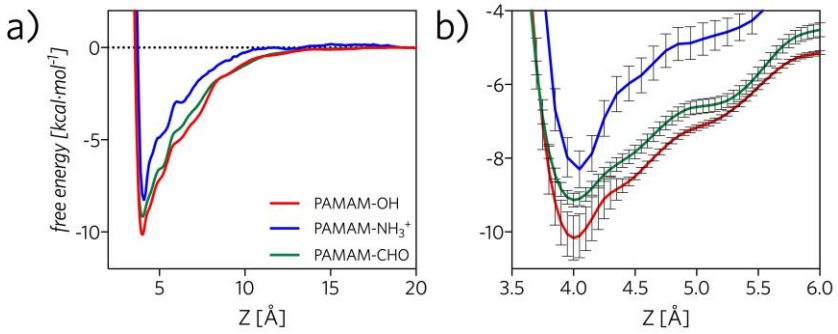

Figure 8: a) 1D free-energy profiles for each dendrimer along the transition coordinate Z. b) Magnification of the global free-energy minima including estimates of the statistical uncertainty (error bars).

When dendrimers' free-energy minima were compared (Figure 8b), PAMAM–OH (-10.2 kcal·mol^{-1}), was shown to be approximately 2 kcal·mol^{-1} more stable than PAMAM–NH_3^+ (-8.2 kcal·mol^{-1}) and 1 kcal·mol^{-1} more stable than PAMAM–CHO (-9.1 kcal·mol^{-1}). Taking into account the experimental evidence of the spontaneous oxidation of PAMAM–OH to PAMAM–CHO in the presence of Au(III), it is probably more appropriate to compare the PAMAM–CHO results to experiment rather than those with PAMAM–OH. The simulations suggest that PAMAM–CHO has a slightly higher affinity for the gold–water interface than PAMAM–NH_3^+, which does not, evidently, translate into better performance as a stabilizing agent. It is likely that the positive charge of the PAMAM–NH_3^+|Au complexes inhibits aggregation, while the neutral PAMAM–CHO|Au complexes are prone to agglomeration.

Previous studies on amino-terminated PAMAM of the second generation reported the interaction free energy with gold nanoparticles using umbrella sampling[69]. Even though gold was not represented with polarizable effects, the value for the protonated system (−8 kcal·mol^{-1}) was quite close to our results. On the other hand, in previous work reported by our group[72], the interaction energy between small gold clusters ($Au_{n=2-8}$ atoms) and PAMAM

G0–OH, $–NH_3^+$ and –CHO systems, was studied using the Density Functional Theory (DFT) approximation, not considering the explicit or implicit introduction of solvent. These results showed stronger binding between gold and PAMAM–NH_3^+, creating complexes with gold nanoclusters 5 kcal·mol^{-1} more stable on average than PAMAM–OH and PAMAM–CHO. However, in aqueous solution, desolvation of the charged NH_3^+ groups likely incurs a greater free energy penalty than desolvation of neutral hydroxyl or aldehyde groups.

Thermodynamic Decomposition of Calculated adsorption Free Energies.

To better understand the role of the solvent and conformational changes in the dendrimer, we decomposed the adsorption free energy into different thermodynamic components. For each dendrimer, we performed a 100 ns simulation (without ABF) in which the coordinate Z was restrained to remain near the position of minimum free energy, beginning from a frame of the ABF calculation consistent with this position. Similar simulations were performed with each dendrimer restrained to a position far from the gold surface (Z=20 Å). From these simulations, we were able to calculate the difference in potential energy between the gold-adsorbed and free states of the dendrimer (ΔU_{total}), which is shown in Table 1.

Table 1: Thermodynamic decomposition of the free energy for adsorption of the dendrimers onto the gold surface.

Potential (kcal/mol)	PAMAM–NH_3^+	PAMAM–OH	PAMAM–CHO
ΔG_{total}	−8.2 ± 0.5	−10.2 ± 0.6	−9.1 ± 0.2
ΔU_{total}	−59.3 ± 0.3	−5.5 ± 0.2	−2.6 ± 0.2
$p\Delta V$	9.1×10^{-3}	1.3×10^{-3}	1.2×10^{-3}
$-T\Delta S_{total}$	51.1 ± 0.6	−4.7 ± 0.6	−6.5 ± 0.4
$\Delta U_{PAMAM–PAMAM}$	21.8 ± 0.1	−1.4 ± 0.1	−0.8 ± 0.1
$\Delta U_{gold–gold}$	1.7 ± 0.1	−0.8 ± 0.1	−0.5 ± 0.1
$\Delta U_{solvent–solvent}$	−74.5 ± 0.3	−18.0 ± 0.2	−19.7 ± 0.2
$\Delta U_{PAMAM–gold}$	−80.3 ± 0.2	−54.0 ± 0.1	−51.9 ± 0.1
$\Delta U_{PAMAM–solvent}$	8.0 ± 0.3	19.1 ± 0.3	22.1 ± 0.3
$\Delta U_{gold–solvent}$	64.0 ± 0.5	50.1 ± 0.3	48.3 ± 0.3

Interestingly, PAMAM–NH_3^+, the charged dendrimer, shows a much more negative change in potential energy than the other two. Adding the pressure–volume work, $p\Delta V$, to ΔU_{total} gives us the total enthalpic contribution to the free energy. We find that $p\Delta V$ is insignificant compared to the other terms and their uncertainties, which is not unusual for molecular binding in aqueous systems[73]; hence, the change in potential energy is essentially the same as the change in enthalpy, $\Delta U_{total} \approx \Delta H_{total}$. The entropic contribution to the adsorption free energy can be calculated by $-T\Delta S_{total} = \Delta G_{total} - \Delta H_{total}$. Both PAMAM–OH and PAMAM–CHO exhibit favorable entropic and enthalpic contributions to their adsorption free energy. We find that adsorption PAMAM–OH is driven by nearly equal contributions of entropy and enthalpy, while the adsorption of PAMAM–CHO has a significantly larger contribution from entropy. PAMAM–NH_3^+ exhibits cancelation between a highly unfavorable entropy term and a highly favorable enthalpy. Invoking the *Van 't Hoff* equation, we predict that the equilibrium constant for adsorption of PAMAM–NH_3^+ onto gold should exhibit a much stronger temperature dependence than the equilibrium constants for adsorption of PAMAM–OH and PAMAM–CHO, owing to the much larger magnitude of ΔH_{total}.

The enthalpic contributions can be further broken down into potential energies acting within and between different subsystems. The lowest free energy configuration of PAMAM–NH_3^+ brings the charged terminal amines closer than they are on average in the unbound dendrimer (see Figure 6b). Hence, there is a markedly unfavorable change in the electrostatic potential energy of the dendrimer upon adsorption ($\Delta U_{PAMAM–PAMAM}$), as indicated in Table 1.

On the other hand, changes in intramolecular energy for PAMAM–OH and PAMAM–CHO upon adsorption to gold are slightly favorable. Given that the positions of the gold atoms are fixed in simulations, the change in intra-gold potential energy ($\Delta U_{gold–gold}$) is entirely due to electrostatic interactions between the charged particles that give polarizability to the gold model. The charged PAMAM–NH_3^+ causes alignment of the gold dipoles in a matter that is slightly energetically unfavorable in the absence of the dendrimer. For the uncharged dendrimers, there is little change in the alignment of the dipoles when the dendrimer absorbs; therefore, $\Delta U_{gold–gold}$ is small in magnitude in these cases. Similar logic can be applied to the electrostatic interactions of the solvent, which is solely water in the case of PAMAM–OH and PAMAM–CHO and water and 4 Cl^- ions in the case of PAMAM–NH_3^+. The presence of the charged solute causes alignment of water molecules and migration of ions in a manner that is unfavorable in the absence of this solute. Placing this charged solute at the water–gold interface rather than in the middle of the water is much

more favorable for the intra-solvent energy ($\Delta U_{\text{solvent–solvent}}$), accounting for a large portion the favorable total enthalpy of PAMAM–NH_3^+ adsorption. $\Delta U_{\text{solvent–solvent}}$ remains favorable for the uncharged dendrimers, but to a much lesser extent. In all cases, the direct interaction between the dendrimer and the gold surface ($\Delta U_{\text{PAMAM–gold}}$) is the largest magnitude enthalpy and highly favorable. However, adsorption of the dendrimer requires desorption of water molecules; hence, favorable $\Delta U_{\text{PAMAM–gold}}$ is partially counteracted by the loss of favorable water–gold interactions ($\Delta U_{\text{gold–solvent}}$). Partial desolvation of the dendrimer, required for adsorption, is also moderately unfavorable ($\Delta U_{\text{PAMAM–solvent}}$).

The above simulations demonstrate that the adsorption thermodynamics of the charged PAMAM–NH_3^+ dendrimer are quite different from the uncharged PAMAM–OH and PAMAM–CHO dendrimers. Adsorption of a single G0 PAMAM–NH_3^+ has a greater ΔG_{total} (weaker affinity) than PAMAM–OH; however, when the particular interaction between the dendrimer and the gold surface is analyzed, the potential energy $\Delta U_{\text{PAMAM–gold}}$ is approximately 30 kcal·mol^{-1} lower compared to the other two dendrimers. This quantity indicates a strong interaction between both interphases, which could play a key role in the stabilization of the gold nanoparticles by the dendrimers. However, due to the charged nature of PAMAM–NH_3^+, there is an unfavorable change in solvent entropy upon adsorption, owing to the substantial rearrangement of water molecules and ions. It should be noted that the above simulations are only roughly representative of the experimental procedure, since they consider PAMAM G0 and the adsorption of a single dendrimer on an isolated gold {111} surface. Although PAMAM G0 has a lower density of terminal groups on its surface than PAMAM G4 and a smaller size, PAMAM G0 is very similar to the terminal branches of PAMAM G4. Studying PAMAM G0 should be sufficient to identify particular atomic-scale interactions with the gold surface and determine the strength of these interactions, while avoiding the computational expense of simulating a full G4 dendrimer. However, solvation effects may differ between PAMAM G4 and PAMAM G0 because the higher density of terminal groups of the G4 dendrimer implies less water accessibility. Overall, the larger PAMAM G4 dendrimers used in the experiments likely show much stronger adsorption to gold than the G0 dendrimers. Furthermore, the surfaces of the gold nanoparticles are likely covered with a sufficiently large density of dendrimers that interactions between multiple dendrimers on the surface become significant.

Conclusions

In the present work, we analyzed the effect of synthesis conditions, gold concentration, and the chemistry of the PAMAM terminal group on the morphology and suspension stability of gold nanoparticles. We conclude that PAMAM–NH_3^+ is superior to PAMAM–OH in producing a stable suspension, with less aggregation. Ultrasound sonication of solutions containing gold salts and PAMAM dendrimers appears to be faster and simpler than mechanical agitation and is preferable if smaller nanoparticles are desired. Our molecular dynamics simulations demonstrate that the gold adsorption thermodynamics of a charged dendrimer like PAMAM–NH_3^+ differ significantly from those of neutral dendrimers like PAMAM–OH. Free-energy calculations in molecular dynamics simulations show that all dendrimers have a high affinity for the gold surface. PAMAM–NH_3^+ has the lowest affinity for the nanoparticle surface; however, when the calculated free energies are decomposed, it can be observed that the adsorption of PAMAM–NH_3^+ to gold is driven by a strong enthalpic component subject to an unfavorable entropic component. The enthalpic component of PAMAM–NH_3^+ is 50 kcal·mol^{-1} less than that the other two dendrimers, which can be related to better stabilization of gold nanoparticles by this dendrimer. Energetically, this term is compensated by a change in entropy owing to the reorganization of water molecules and ions due to the charged nature of the dendrimer.

Acknowledgements

M.B.C. is grateful to Fondecyt for funding support (Project Nº 1180023). Powered@NLHPC: This research was partially supported by the supercomputing infrastructure of the NLHPC (ECM-02). H.P. thanks to Fondecyt grant No. 1171155, also, to the Millennium Nucleus of Ion Channels-Associated Diseases (MiNICAD) is a Millennium Nucleus supported by the Iniciativa Científica Milenio of the Ministry of Economy, Development and Tourism (Chile). This material is based upon work supported by the National Science Foundation (USA) under grant number CHE-1726332.

Supporting Information. UV-vis spectra of the synthetized nanoparticles in the absence of reducing agent and AFM images of gold nanoparticles.

References

1. Zhang, L.; Gu, F.; Chan, J.; Wang, A.; Langer, R.; Farokhzad, O., Nanoparticles in medicine: therapeutic applications and developments. *Clinical pharmacology and therapeutics* **2008,** *83* (5), 761-769.
2. Xu, Y. Y.; Bian, C.; Chen, S.; Xia, S., A microelectronic technology based amperometric immunosensor for α-fetoprotein using mixed self-assembled monolayers and gold nanoparticles. *Anal. Chim. Acta* **2006,** *561* (1), 48-54.
3. Ayati, A.; Ahmadpour, A.; Bamoharram, F. F.; Tanhaei, B.; Mänttäri, M.; Sillanpää, M., A review on catalytic applications of Au/TiO 2 nanoparticles in the removal of water pollutant. *Chemosphere* **2014,** *107*, 163-174.
4. Dinali, R.; Ebrahiminezhad, A.; Manley-Harris, M.; Ghasemi, Y.; Berenjian, A., Iron oxide nanoparticles in modern microbiology and biotechnology. *Critical Reviews in Microbiology* **2017**, 1-15.
5. Jin, R.; Charles Cao, Y.; Hao, E.; Metraux, G. S.; Schatz, G. C.; Mirkin, C. A., Controlling anisotropic nanoparticle growth through plasmon excitation. *Nature* **2003,** *425* (6957), 487-490.
6. Roduner, E., Size matters: why nanomaterials are different. *Chem. Soc. Rev.* **2006,** *35* (7), 583-592.
7. Lewis, L. N., Chemical catalysis by colloids and clusters. *Chemical Reviews* **1993,** *93* (8), 2693-2730.
8. Sauter, C.; Emin, M. A.; Schuchmann, H. P.; Tavman, S., Influence of hydrostatic pressure and sound amplitude on the ultrasound induced dispersion and de-agglomeration of nanoparticles. *Ultrasonics Sonochemistry* **2008,** *15* (4), 517-523.
9. Grillo, R.; Rosa, A. H.; Fraceto, L. F., Engineered nanoparticles and organic matter: A review of the state-of-the-art. *Chemosphere* **2015,** *119*, 608-619.
10. Crooks, R. M.; Zhao, M.; Sun, L.; Chechik, V.; Yeung, L. K., Dendrimer-encapsulated metal nanoparticles: synthesis, characterization, and applications to catalysis. *Accounts of chemical research* **2001,** *34* (3), 181-190.
11. Tomalia, D. A.; Baker, H.; Dewald, J.; Hall, M.; Kallos, G.; Martin, S.; Roeck, J.; Ryder, J.; Smith, P., A new class of polymers-starburst-dendritic macromolecules. *Polym. J.* **1985,** *17*, 117-132.
12. Fréchet, J. M. J.; Tomalia, D. A., *Dendrimers and Other Dendritic Polymers.* John Wiley & Sons: Chichester, New York, USA, 2001.
13. Scott, R. W.; Wilson, O. M.; Crooks, R. M., Synthesis, characterization, and applications of dendrimer-encapsulated nanoparticles. ACS Publications: 2005.
14. Cakara, D.; Kleimann, J.; Borkovec, M., Microscopic Protonation Equilibria of Poly(amidoamine) Dendrimers from Macroscopic Titrations. *Macromolecules* **2003,** *36* (11), 4201-4207.
15. Karatasos, K.; Posocco, P.; Laurini, E.; Pricl, S., Poly(amidoamine)-based Dendrimer/siRNA Complexation Studied by Computer Simulations: Effects of pH and Generation on Dendrimer Structure and siRNA Binding. *Macromolecular Bioscience* **2012,** *12* (2), 225-240.
16. Shen, Y.; Zhou, Z.; Sui, M.; Tang, J.; Xu, P.; Kirk, E. A. V.; Murdoch, W. J.; Fan, M.; Radosz, M., Charge-reversal polyamidoamine dendrimer for cascade nuclear drug delivery. *Nanomedicine* **2010,** *5* (8), 1205-1217.
17. Borodko, Y.; Thompson, C. M.; Huang, W.; Yıldız, H. B.; Frei, H.; Somorjai, G. A., Spectroscopic study of platinum and rhodium dendrimer (PAMAM G4OH) compounds: structure and stability. **2011**.
18. Balogh, L.; Tomalia, D. A., Poly(Amidoamine) Dendrimer-Templated Nanocomposites. 1. Synthesis of Zerovalent Copper Nanoclusters. *J. Am. Chem. Soc.* **1998,** *120* (29), 7355-7356.

19. Boyen, H.-G.; Kästle, G.; Weigl, F.; Koslowski, B.; Dietrich, C.; Ziemann, P.; Spatz, J. P.; Riethmüller, S.; Hartmann, C.; Möller, M.; Schmid, G.; Garnier, M. G.; Oelhafen, P., Oxidation-Resistant Gold-55 Clusters. *Science* **2002,** *297* (5586), 1533-1536.
20. Burda, C.; Chen, X.; Narayanan, R.; El-Sayed, M. A., Chemistry and Properties of Nanocrystals of Different Shapes. *Chemical Reviews* **2005,** *105* (4), 1025-1102.
21. Fernandez, C. A.; Wai, C. W., A Simple and Rapid Method of Making 2D and 3D Arrays of Gold Nanoparticles. *Journal of Nanoscience and Nanotechnology* **2006,** *6* (3), 669-674.
22. Orlando, A.; Colombo, M.; Prosperi, D.; Corsi, F.; Panariti, A.; Rivolta, I.; Masserini, M.; Cazzaniga, E., Evaluation of gold nanoparticles biocompatibility: a multiparametric study on cultured endothelial cells and macrophages. *J. Nanopart. Res.* **2016,** *18* (3), 1-12.
23. Kim, J. M.; Sohn, S. H.; Han, N. S.; Park, S. M.; Kim, J.; Song, J. K., Blue Luminescence of Dendrimer-Encapsulated Gold Nanoclusters. *ChemPhysChem* **2014,** *15* (14), 2917-2921.
24. Yancey, D. F.; Chill, S. T.; Zhang, L.; Frenkel, A. I.; Henkelman, G.; Crooks, R. M., A theoretical and experimental examination of systematic ligand-induced disorder in Au dendrimer-encapsulated nanoparticles. *Chemical Science* **2013,** *4* (7), 2912-2921.
25. Frankamp, B. L.; Boal, A. K.; Rotello, V. M., Controlled Interparticle Spacing through Self-Assembly of Au Nanoparticles and Poly(amidoamine) Dendrimers. *J. Am. Chem. Soc.* **2002,** *124* (51), 15146-15147.
26. Camarada, M., DFT investigation of the interaction of gold nanoclusters with poly (amidoamine) PAMAM G0 dendrimer. *Chemical Physics Letters* **2016,** *654*, 29-36.
27. Knecht, M. R.; Weir, M. G.; Myers, V. S.; Pyrz, W. D.; Ye, H.; Petkov, V.; Buttrey, D. J.; Frenkel, A. I.; Crooks, R. M., Synthesis and characterization of Pt dendrimer-encapsulated nanoparticles: effect of the template on nanoparticle formation. *Chem. Mater.* **2008,** *20* (16), 5218-5228.
28. Scott, R. W.; Ye, H.; Henriquez, R. R.; Crooks, R. M., Synthesis, characterization, and stability of dendrimer-encapsulated palladium nanoparticles. *Chem. Mater.* **2003,** *15* (20), 3873-3878.
29. Esumi, K.; Suzuki, A.; Aihara, N.; Usui, K.; Torigoe, K., Preparation of gold colloids with UV irradiation using dendrimers as stabilizer. *Langmuir* **1998,** *14* (12), 3157-3159.
30. Garcia, M. E.; Baker, L. A.; Crooks, R. M., Preparation and characterization of dendrimer− gold colloid nanocomposites. *Anal. Chem.* **1999,** *71*, 256.
31. Shi, X.; Sun, K.; Baker, J. R., Spontaneous Formation of Functionalized Dendrimer-Stabilized Gold Nanoparticles. *J. Phys. Chem. C* **2008,** *112*, 8251.
32. Melinger, J. S.; Kleiman, V. D.; McMorrow, D.; Gröhn, F.; Bauer, B. J.; Amis, E., Ultrafast Dynamics of Gold-Based Nanocomposite Materials. *J. Phys. Chem. A* **2003,** *107*, 3424.
33. Garcia-Martinez, J. C.; Crooks, R. M., Extraction of Au Nanoparticles Having Narrow Size Distributions from within Dendrimer Templates. *J. Am. Chem. Soc.* **2004,** *126*, 16170.
34. Gröhn, F.; Bauer, B. J.; Akpalu, Y. A.; Jackson, C. L.; Amis, E. J., Dendrimer Templates for the Formation of Gold Nanoclusters. *Macromolecules* **2000,** *33*, 6042.
35. Balogh, L.; Valluzzi, R.; Laverdure, K. S.; Gido, S. P.; Hagnauer, G. L.; Tomalia, D. A., Formation of silver and gold dendrimer nanocomposites. *J. Nanopart. Res.* **1999,** *1*, 353.
36. Hoffman, L. W.; Andersson, G. G.; Sharma, A.; Clarke, S. R.; Voelcker, N. H., New Insights into the Structure of PAMAM Dendrimer/Gold Nanoparticle Nanocomposites. *Langmuir* **2011,** *27* (11), 6759-6767.
37. Zheng, J.; Stevenson, M. S.; Hikida, R. S.; Van Patten, P. G., Influence of pH on Dendrimer-Protected Nanoparticles. *J. Phys. Chem. B* **2002,** *106* (6), 1252-1255.

38. Kim, Y. G.; Oh, S. K.; Crooks, R. M., Preparation and characterization of 1− 2 nm dendrimer-encapsulated gold nanoparticles having very narrow size distributions. *Chem. Mater.* **2004,** *16*, 167.
39. West, R.; Wang, Y.; Goodson, T., Nonlinear Absorption Properties in Novel Gold Nanostructured Topologies. *J. Phys. Chem. B* **2003,** *107* (15), 3419-3426.
40. Esumi, K.; Hosoya, T.; Suzuki, A.; Torigoe, K., Spontaneous Formation of Gold Nanoparticles in Aqueous Solution of Sugar-Persubstituted Poly(amidoamine)dendrimers. *Langmuir* **2000,** *16* (6), 2978-2980.
41. Kim, Y.-G.; Oh, S.-K.; Crooks, R. M., Preparation and characterization of 1-2 nm dendrimer-encapsulated gold nanoparticles having very narrow size distributions. *Chem. Mater.* **2004,** *16* (1), 167-172.
42. Humphrey, W.; Dalke, A.; Schulten, K., VMD - Visual Molecular Dynamics. *J. Molec. Graphics* **1996,** *14*, 33-38.
43. Vanommeslaeghe, K.; Hatcher, E.; Acharya, C.; Kundu, S.; Zhong, S.; Shim, J.; Darian, E.; Guvench, O.; Lopes, P.; Vorobyov, I.; Mackerell, A. D., CHARMM general force field: A force field for drug-like molecules compatible with the CHARMM all-atom additive biological force fields. *Journal of Computational Chemistry* **2010,** *31* (4), 671-690.
44. Vanommeslaeghe, K.; MacKerell, A. D., Automation of the CHARMM General Force Field (CGenFF) I: Bond Perception and Atom Typing. *Journal of Chemical Information and Modeling* **2012,** *52* (12), 3144-3154.
45. Vanommeslaeghe, K.; Raman, E. P.; MacKerell, A. D., Automation of the CHARMM General Force Field (CGenFF) II: Assignment of Bonded Parameters and Partial Atomic Charges. *Journal of Chemical Information and Modeling* **2012,** *52* (12), 3155-3168.
46. Rosa, M.; Corni, S.; Di Felice, R., A density functional theory study of cytosine on Au (111). *J. Phys. Chem. C* **2012,** *116* (40), 21366-21373.
47. Wright, L. B.; Rodger, P. M.; Corni, S.; Walsh, T. R., GolP-CHARMM: first-principles based force fields for the interaction of proteins with Au (111) and Au (100). *Journal of chemical theory and computation* **2013,** *9* (3), 1616-1630.
48. Phillips, J. C.; Braun, R.; Wang, W.; Gumbart, J.; Tajkhorshid, E.; Villa, E.; Chipot, C.; Skeel, R. D.; Kalé, L.; Schulten, K., Scalable molecular dynamics with NAMD. *Journal of Computational Chemistry* **2005,** *26* (16), 1781-1802.
49. Martyna, G. J.; Tobias, D. J.; Klein, M. L., *J. Chem. Phys.* **1994,** *101*, 4177–4189.
50. Darden, T.; York, D.; Pedersen, L. J., *Chem. Phys. Lett.* **1993,** *98*, 10089–10092.
51. Jorgensen, W. L.; Chandrasekhar, J.; Madura, J. D.; Impey, R. W.; Klein, M. L., Comparison of simple potential functions for simulating liquid water. *J. Chem. Phys.* **1983,** *79* (2), 926-935.
52. MacKerell, J., A. D. ; Bashford, D.; Bellott, M.; Dunbrack Jr., R. L.; Evanseck, J. D.; Field, M. J.; Fischer, S.; Gao, J.; Guo, H.; Ha, S.; Joseph-McCarthy, D.; Kuchnir, L.; Kuczera, K.; Lau, F. T. K.; Mattos, C.; Michnick, S.; Ngo, T.; Nguyen, D. T.; Prodhom, B.; Reiher, I., W.E.; Roux, B.; Schlenkrich, M.; Smith, J. C.; Stote, R.; Straub, J.; Watanabe, M.; Wiorkiewicz-Kuczera, J.; Yin, D.; Karplus, M., *J. Phys. Chem. B* **1998,** *102*, 3586-3616.
53. Beglov, D.; Roux, B., *Journal of Chemical Physics* **1994,** *100*, 9050-9063.
54. Settle, M., An analytical version of the SHAKE and RATTLE algorithm for rigid water molecules. *J. Comput. Chem* **1992,** *13*, 952-962.
55. Andersen, H. J., *Comp. Phys.* **1983,** *52*, 24–34.
56. Comer, J.; Gumbart, J. C.; Hénin, J.; Lelièvre, T.; Pohorille, A.; Chipot, C., The adaptive biasing force method: Everything you always wanted to know but were afraid to ask. *J. Phys. Chem. B* **2014,** *119* (3), 1129-1151.
57. Darve, E.; Pohorille, A., Calculating free energies using average force. *J. Chem. Phys.* **2001,** *115* (20), 9169-9183.

58. Hénin, J.; Chipot, C., Overcoming free energy barriers using unconstrained molecular dynamics simulations. *J. Chem. Phys.* **2004,** *121* (7), 2904-2914.
59. Fiorin, G.; Klein, M. L.; Hénin, J., Using collective variables to drive molecular dynamics simulations. *Mol. Phys.* **2013,** *111* (22-23), 3345-3362.
60. Aschwanden, L.; Mallat, T.; Krumeich, F.; Baiker, A., A simple preparation of an efficient heterogeneous gold catalyst for aerobic amine oxidation. *J. Mol. Catal. A: Chem.* **2009,** *309* (1), 57-62.
61. Pina, C. D.; Falletta, E.; Rossi, M., Selective oxidation of tertiary amines on gold catalysts. *Top. Catal.* **2007,** *44* (1), 325-329.
62. Yonezawa, T.; Matsune, H.; Kunitake, T., Layered nanocomposite of close-packed gold nanoparticles and TiO2 gel layers. *Chem. Mater.* **1999,** *11* (1), 33-35.
63. Doremus, R. H.; Rao, P., Optical properties of nanosized gold particles. *J. Mater. Res.* **1996,** *11* (11), 2834-2840.
64. Mie, G., Beiträge zur Optik trüber Medien, speziell kolloidaler Metallösungen. *Annalen der physik* **1908,** *330* (3), 377-445.
65. Martin, C. R., Nanomaterials: A Membrane-Based Synthetic Approach. *Science* **1994,** *266* (5193), 1961.
66. Schneider, C. A.; Rasband, W. S.; Eliceiri, K. W., NIH Image to ImageJ: 25 years of image analysis. *Nature methods* **2012,** *9* (7), 671-675.
67. Yonezawa, Y.; Kawabata, I.; Sato, T., Photochemical formation of colloidal gold particles in chitosan films. *Berichte der Bunsengesellschaft für physikalische Chemie* **1996,** *100* (1), 39-45.
68. Giorgetti, E.; Giusti, A.; Giammanco, F.; Marsili, P.; Laza, S., Dendrimer-capped nanoparticles prepared by picosecond laser ablation in liquid environment. *Molecules* **2009,** *14* (9), 3731-3753.
69. Mandal, T.; Dasgupta, C.; Maiti, P. K., Engineering gold nanoparticle interaction by PAMAM dendrimer. *J. Phys. Chem. C* **2013,** *117* (26), 13627-13636.
70. Comer, J.; Phillips, J. C.; Schulten, K.; Chipot, C., Multiple-Replica Strategies for Free-Energy Calculations in NAMD: Multiple-Walker Adaptive Biasing Force and Walker Selection Rules. *Journal of Chemical Theory and Computation* **2014,** *10* (12), 5276-5285.
71. Minoukadeh, K.; Chipot, C.; Lelièvre, T., Potential of Mean Force Calculations: A Multiple-Walker Adaptive Biasing Force Approach. *Journal of Chemical Theory and Computation* **2010,** *6* (4), 1008-1017.
72. Camarada, M. B., PAMAM Dendrimers as Support for the Synthesis of Gold Nanoparticles: Understanding the Effect of the Terminal Groups. *J. Phys. Chem. A* **2017,** *121* (42), 8124-8135.
73. Hansen, N.; van Gunsteren, W. F., Practical Aspects of Free-Energy Calculations: A Review. *Journal of Chemical Theory and Computation* **2014,** *10* (7), 2632-2647.